Corrosion Science 52 (2010) 1649–1659

Contents lists available at ScienceDirect

Corrosion Science

journal homepage: www.elsevier.com/locate/corsci

Electrochemical investigation of chloride-induced depassivation of black steel rebar under simulated service conditions

P. Ghods [a], O.B. Isgor [a,*], G.A. McRae [a], G.P. Gu [b]

[a] Carleton University, Ottawa, Ontario, Canada
[b] CANMET Materials Technology Laboratory, Ottawa, Ontario, Canada

ARTICLE INFO

Article history:
Received 1 September 2009
Accepted 6 February 2010
Available online 15 February 2010

Keywords:
A. Steel reinforced concrete
A. Concrete
B. EIS
B. Polarization
C. Passive films
C. Pitting corrosion

ABSTRACT

Electrochemical measurements of chloride thresholds are reported in simulated concrete pore solution for as-received and surface-modified rebar in an experimental apparatus designed to simulate service conditions. Surface modification led to higher chloride thresholds and reduced variability. The variability in thresholds for as-received rebar was represented by a log-normal distribution; therefore, simple averages of chloride thresholds, without reference to underlying distribution, might not provide reliable indicators of depassivation. The relative constancy of electrochemical measurements below thresholds, and the dependence of the thresholds on surface conditions, suggests that rebar depassivation is likely caused by local critical chemical conditions at the steel surface.

1. Introduction

Within the high alkaline environment of concrete (pH > 12.5), black steel rebar is generally well protected against corrosion by a passive oxide film. The partial or complete loss of the passive layer, known as depassivation, may lead to excessive rates of corrosion and premature failure of reinforced concrete structures. Chlorides are well known to cause depassivation, if they are present in sufficient concentration, however, reported values of threshold chloride concentrations for rebar depassivation in concrete cover a wide range and have a large degree of uncertainty [1,2]. Understanding the underlying variability in threshold values is important for service-life-based design and for the prediction of the remaining service life of concrete structures.

Currently, there is no comprehensive explanation for the variability of measured chloride-depassivation thresholds (henceforth "chloride thresholds"), but it is believed to depend on a large number of factors: the alkalinity of the pore solution [3–9]; the presence of auxiliary ions such as sulphates, sodium and potassium [10–16]; rebar surface conditions [6,8,17]; the properties of the rebar-concrete interface [18,19]; chloride binding in concrete [20–22]; and oxygen availability around the reinforcement [5,18,22–24].

Experimental studies to isolate the mechanism of chloride depassivation of black steel rebar in concrete are challenging because it is difficult to control confounding variables, because of the long waiting times (months) required due to the slow ingress of chloride into concrete, and because of the difficulty in measuring chloride concentrations in the vicinity of the rebar surface. Therefore, most experimental studies of chloride thresholds have been done using relatively small-scale bench-top devices in which the sections of rebar are submerged in solutions that simulate the chemical environment most often found in extracted pore solutions. These bench-top experiments usually include standard electrochemical procedures, which can be done relatively quickly under conditions for which the control of variables is relatively easy; thus, bench-top experiments are widely used to study chloride threshold of steel in concrete. However, it is often difficult to relate the results of these experiments to rebar in service.

For example, a portion of chloride threshold data have been obtained from laboratory experiments in simulated solutions on highly-processed (e.g. polished and/or pickled) steel specimens or on relatively small exposure surfaces (typically smaller than 2 cm^2), that were machined from rebar samples [4,10,25–27]. These experiments provide information on the effects of solution chemistry on the pristine steel surface, but, because the surfaces are processed to eliminate the deformities (ribbing), defects and mill-scale found in service conditions, these experiments are not ideal to draw practical conclusions about rebar depassivation in concrete [6,8,28,29]. Fortunately, it is not necessary to test rebar of lengths typically used in service, which can be several meters, because the resistivity of concrete is relatively high (typically larger than 100 Ω-m), so that the electrochemical processes on the re-

* Corresponding author. Tel.: +1 613 5202600x2984; fax: +1 613 520 3951.
E-mail address: burkan_isgor@carleton.ca (O.B. Isgor).

0010-938X/$ - see front matter © 2010 Elsevier Ltd. All rights reserved.
doi:10.1016/j.corsci.2010.02.016

bar surface take place on a scale of several centimetres [30]. Hence, rebar specimens of a few centimetres provide representative lengths, provided they are long enough to contain sufficient sampling of all the surface characteristics (e.g. ribbing, defects and mill-scale).

Cutting specimens to lengths of a few centimetres introduces freshly cut surfaces that are relatively large fractions of the total specimen surface area. These freshly cut surfaces will most likely have a different and confounding chloride threshold, so some care must be taken to isolate the ends of the specimens. Effective coating of the ends would eliminate this problem; however, our initial attempts to coat the ends with a non-conductive epoxy were foiled by corrosion in the crevices between the rebar and the epoxy in the presence of chloride. Similar difficulties have been reported by others [8,18,31]. In this study, we report a method to coat the cut ends of rebar specimens that effectively eliminates crevice corrosion.

The cylindrical nature of rebar suggests that the standard flat counter electrodes used in most other studies, in which the specimens are generally small, polished and flat, be replaced with a co-axial cylindrical electrode. This co-axial geometry provides a relatively uniform radial electric field at the rebar surface. Thus, in this study, we introduce an experimental electrochemical setup in which a short section of as-received rebar, coated at both ends, is immersed in simulated concrete pore solution, and surrounded by a co-axial counter electrode. In addition, in our study the reference electrode was connected by a very small glass tip that was designed to minimize the distortion of the electric field.

The main objective of this paper is to measure chloride thresholds of black steel rebar under conditions reasonably comparable with those found in service conditions. Various electrochemical techniques are used to follow passivation and depassivation of as-received rebar specimens, with and without surface modification, in simulated pore solutions as a function of chloride concentration. A previous study [16] has shown the importance of pore solution composition for the passivation of rebar; in the current study, this result is extended to depassivation. The electrochemical techniques will include free corrosion potential (FCP) measurements, electrochemical impedance spectroscopy (EIS), linear polarization resistance (LPR) and anodic polarization (AP). In addition, some suggestions will be provided on how to report chloride thresholds in terms of probabilities.

The writers acknowledge that concrete provides a different environment for reinforcing steel from that of simulated pore solution. The reserve alkalinity of concrete originating from the hydration products of cement, the presence of alkalis and other chemical compounds, and the pore structure of concrete are mainly responsible for this difference. Among these factors, the pore structure of concrete plays an important role: First, it creates a unique mass transport pattern for the ions in the concrete pore solution. Second, the individual pores may act as micro-environments that may show significant variation in chemical composition when compared with the bulk medium. Both of these factors can enable changes in the local chemistry of the pores to occur, hence, affect the depassivation and corrosion mechanisms of steel in concrete. The study of these confounding factors is not within the scope of this research.

2. Experimental setup

2.1. Synthetic pore solution

Two synthetic solutions were used in this study to simulate the pore solutions found in concrete. The label "CH" refers to a saturated calcium hydroxide solution, where "C" stands for calcium and "H" stands for hydroxide; this is typically used as a pore solution surrogate. The solution referred as "CP", where "C" stands for concrete and "P" stands for pore, was prepared with typical concentrations of different anions and cations that can be found in ordinary portland cement concrete (OPC) pore solution [32–35]. The CP solution contains small amounts of sulphate ions at the level that is typically present in concrete pore solutions. In Table 2, the concentrations of the different compounds that have been added to distilled water to produce the CP solution are presented. The actual concentrations of the anions and cations in solution were measured using Inductively Coupled Plasma-Atomic Emission Spectroscopy (ICP-AES) (Model: Varian Vista RL).

2.2. Sample preparation

Two types of specimens were prepared for this study: as-received and 'turned-and-polished'. Both specimen types were cut to 30 mm lengths from deformed black steel rebar of 10 mm nominal diameter. The as-received surfaces were not prepared further. The turned-and-polished specimens were turned on a lathe to remove the deformities and the mill-scale, and then ground to 600 Grit. The average area of the exposed rebar surfaces was $10.6 \pm 0.2\ cm^2$, which was chosen in accordance with the recommendations of Li and Sagues [28]. The elemental composition of the black steel used in this study is shown in Table 1.

Table 1
Steel elemental composition.

Element	Weight %
C	0.26
Si	0.27
Mn	1.10
Cr	0.05
Ni	0.07
Mo	<0.01
Cu	0.21
Al	<0.005
Nb	<0.01
V	<0.005
Ti	<0.005
B	<0.0005
P	0.01
S	0.03
W	<0.01
Sn	0.021
Co	0.01
Zr	<0.01
Fe	Balance

Table 2
Concentrations of the species in the two test solutions (CP and CH).

Solution	Added compounds (M)				Measured ions (mg/l)				pH	σ^* (mS/cm)	$Do_2{}^{**}$(mg/l)
	$Ca(OH)_2$	Na(OH)	K(OH)	$CaSO_4$	Ca^{2+}	Na^+	K^+	SO_4^{2-}			
CP	0.1	0.1	0.2	0.003	3	2232	8059	277	13.3	64.9	2.27
CH	0.1	0	0	0	814	3	0.4	2	12.5	8.82	2.28

* Conductivity of the solution.
** Dissolved oxygen.

The ends of the rebar specimens were isolated to avoid the confounding effects of freshly cut surfaces, and in a way that was not susceptible to crevice corrosion. Initial attempts to eliminate crevice corrosion by coating the ends with epoxy or silicon glue proved unsuccessful. It was found that a Teflon washer held tight to the surface by plastic screws fitted into threaded holes machined into the specimen ends, as shown schematically in Fig. 1, eliminated all visible signs of crevice corrosion in this study. The top screw had a hole drilled axially in the middle to accommodate a steel wire (Alloy: ER316L, Diameter: 0.9 mm) that was spot welded to the bottom of the threaded hole and encased in a plastic tube (see Fig. 1b).

2.3. Co-axial corrosion cell

The cylindrical geometry of the rebar was complemented with a co-axial platinum mesh counter electrode that was used to produce a uniformly-distributed electric field around the exposed surface of the rebar specimens. The mesh counter electrode was longer than the rebar specimens as indicated in Fig. 2. The reference potential was provided by a saturated calomel electrode (SCE) placed in the port connected to the main body of the cell. The port was linked to the test region by a glass tube that terminated with a thin tip situated between the working and counter electrodes, and 5 mm away from the surface of the specimens.

3. Experimental program

A number of standard electrochemical techniques were used to determine chloride thresholds for the depassivation of the surface oxide films on rebar: free corrosion potential (FCP), electrochemical impedance spectroscopy (EIS), linear polarization resistance (LPR) and anodic polarization (AP).

The rebar specimens were passivated in two beakers containing the CP solution and another two containing the CH solution. In each beaker, 24 as-received and 24 turned-and-polished rebar specimens were immersed for 2 weeks. The immersion time was selected based on the results of previous tests that have shown at least 8 days is required to achieve stable passive films on rebar surfaces [16,36].

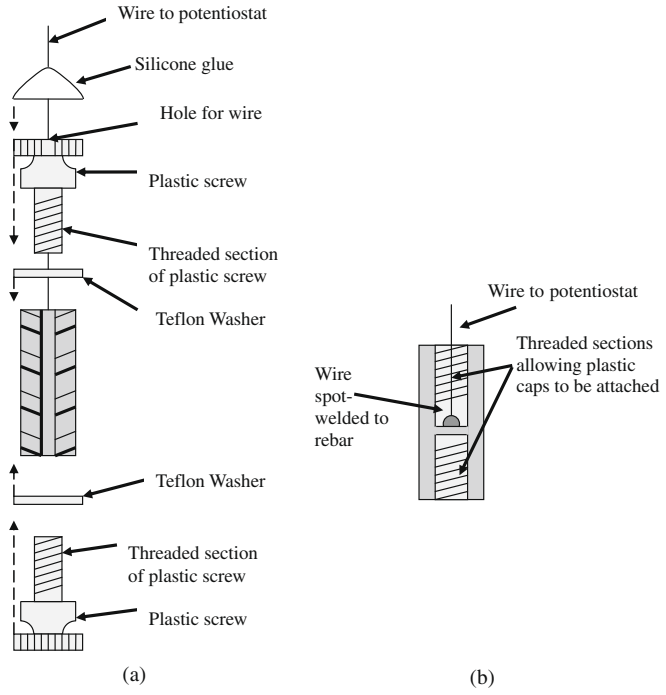

Fig. 1. Schematic illustration of rebar specimen: (a) Pull-out diagram, (b) cross section.

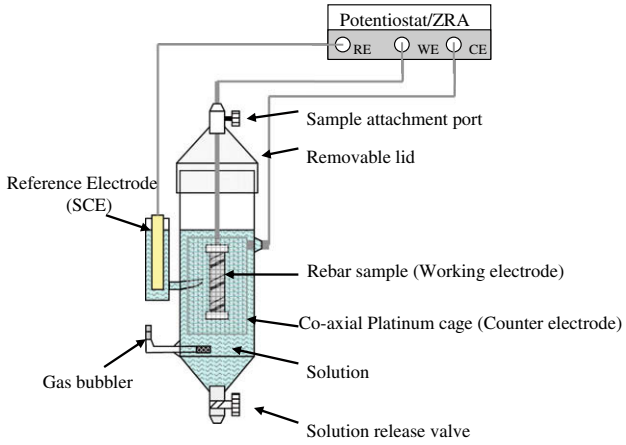

Fig. 2. Schematic illustration of the co-axial corrosion cell.

After the initial 2-week passivation, the chloride concentrations in the solutions were increased at 7-day intervals for 2 months (1400 h), as shown in Table 3, by adding sodium chloride (NaCl, reagent grade) and stirring. Before each chloride addition, three replicate specimens of each type (as-received and turned-and-polished) were removed and then immersed in the same solution in the co-axial corrosion cell for sequential examination by EIS, LPR, and AP. In parallel, the free corrosion potentials of other rebar specimens in the CP and CH solutions were monitored continuously. The pH, conductivity and dissolved oxygen of the solutions were measured with a VWR SympHony SP90M5 before and after each chloride addition; there were no significant changes in these parameters during the tests; the averages of these measurements are presented in Table 2. Further details of all the tests carried out in the study are presented in the following sections.

3.1. Free corrosion potential (FCP)

A sudden drop of FCP of the rebar in the simulated pore solutions is a simple indication of depassivation. The FCP in the passive state is generally between −100 mV(SCE) and −200 mV(SCE), whereas after complete depassivation, it drops below −350 mV(SCE). In this study, free corrosion potentials of three replicate as-received rebar specimens in the CP and CH solutions, and three replicate turned-and-polished samples in the CP solution, were recorded at 60-s intervals using a Gamry PC4/300 Potentiostat/Galvanosatat/ZRA and a Gamry Multiplexer. A saturated calomel electrode (Model: Accumet) was used as a reference electrode.

3.2. Electrochemical impedance spectroscopy (EIS)

EIS tests were carried out on replicate rebar specimens (i.e., 3 replicate as-received specimens that were immersed in the CH solution, 3 as-received from the CP solution, and 3 turned-and-polished specimens from the CP solution) 7 days after each chloride addition, using a Gamry PC4/300 Potentiostat/Galvanosatat/ZRA. To avoid extensive exposure to air, rebar specimens were transferred within seconds from the breakers to the co-axial corrosion cell, which contained the same solution. The FCP was measured for 60 min before the EIS measurement to ensure the stability of the electrochemical system. If the FCP varied more than 10 mV over an hour, the measurement was postponed until the potential

Table 3
The concentration of total chloride at each 7-day interval of the test for two solutions. These intervals correspond to the incremental shading used in Figs. 3–5.

Surface condition	Solution	Chloride addition increments (M)							
		Start	1st	2nd	3rd	4th	5th	6th	7th
As-received	CP	0	0.03	0.05	0.1	0.15	0.3	0.5	1
	CH	0	0.003	0.005	0.01	0.02	0.05	0.1	0.3
Turned-and-Polished	CP	0	0.01	0.05	0.45	1.25	2	3	–

stabilized. The EIS measurements were done at the free potential, with an AC voltage of 10 mV RMS, between 10^5 and 10^{-3} Hz at 10 equally spaced frequencies per decade.

3.3. Linear polarization resistance (LPR)

After completion of each EIS test, LPR measurements were conducted on each specimen without modification of the experimental arrangement with a Gamry PC4/300 Potentiostat/Galvanosatat/ZRA. The FCP was monitored for 60 min before the LPR measurement to ensure the stability of the electrochemical system, and if it varied by more than 10 mV, the measurement was postponed until the potential stabilized. The LPR measurements started 15 mV below, and ended 15 mV above, the FCP of each specimen. The scan rate was 0.166 mV/s, as prescribed in ASTM G5 [37]. Slower scan rates did not affect the results, which is in accord with earlier work [10,38].

3.4. Anodic polarization (AP)

After the LPR measurements, anodic polarization curves of each specimen were obtained without modification of the experimental arrangement using a Gamry PC4/300 Potentiostat/Galvanostat/ZRA. As for the EIS and LPR measurements, the FCP was monitored for 60 min before the EIS test to ensure stability. The AP measurements started at the FCP for each specimen. The potentials were raised to 600 mV(SCE) in the forward (anodic) direction, and then lowered to −100 mV(SCE) below the FCP in the backward (cathodic) direction. The scan rate in both directions was 0.166 mV/s, which is as prescribed by ASTM G5 [37]. The choice of scan rate is a compromise between accuracy and the time to complete the measurement. It was found in this study that slower scan rates did not change the results, which is consistent with other studies [10,38,39].

4. Results

In this section, we describe the results of four electrochemical techniques used to determine chloride thresholds. In each case, negligible changes were observed in the electrochemical responses up to a certain chloride concentration. Upon further addition of chloride (as per Table 3) large changes were observed followed by visible pits on the rebar surfaces. These changes define chloride thresholds for rebar: reported chloride thresholds in this section are thus upper limits for the chloride concentrations associated with the large change.

4.1. FCP results

Figs. 3 and 4 present the FCP measurements, as averages of three replicate as-received specimens, in the CP and CH solutions, respectively. Fig. 5 presents the FCP measurements, as averages of three replicate turned-and-polished specimens, in the CP solution. In all cases, the FCP increases gradually during the early stages of immersion and becomes relatively constant after approximately 10 days (i.e., 240 h). This is consistent with earlier studies that showed the passive film on rebar stabilizes after approximately 10 days [16,36].

Once the passive films stabilized, the average FCP of the as-received rebar was −169 mV(SCE) (see Fig. 3) in the CP solution, and −156 mV(SCE) (see Fig. 4) in the CH solution. The average FCP of the turned-and-polished rebar specimens in the CP solution after stabilization was −220 mV(SCE) (Fig. 5), which is significantly

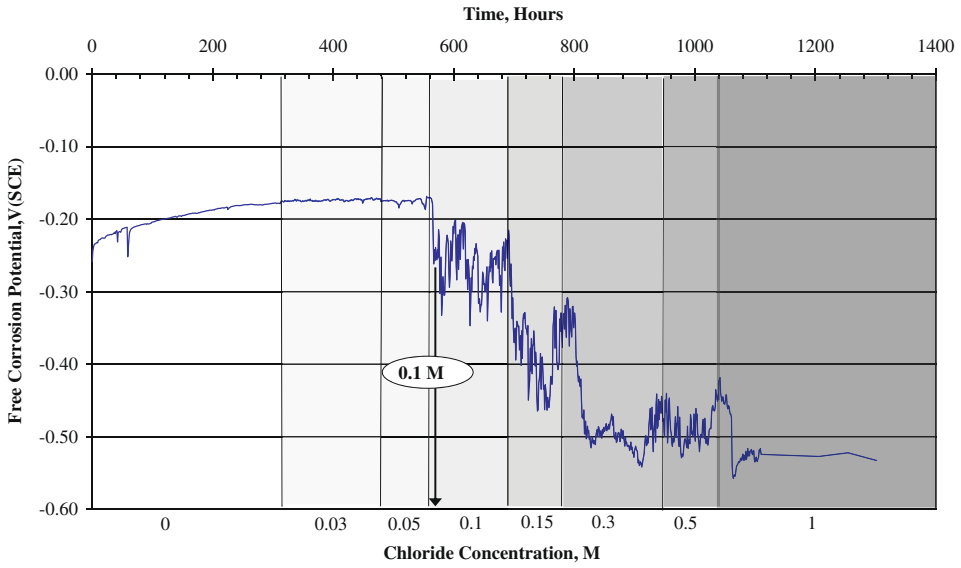

Fig. 3. Average free corrosion potential of three as-received rebars in the CP solution. Shading in the figure corresponds to the increments of chloride addition in Table 3.

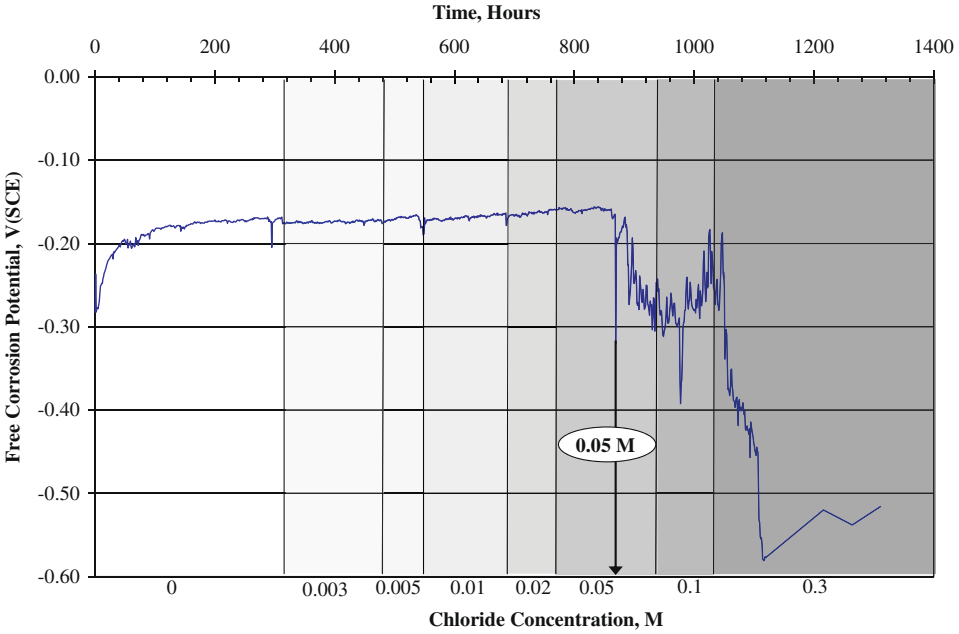

Fig. 4. Average free corrosion potential of three as-received rebars in the CH solution. Shading in the figure corresponds to the increments of chloride addition in Table 3.

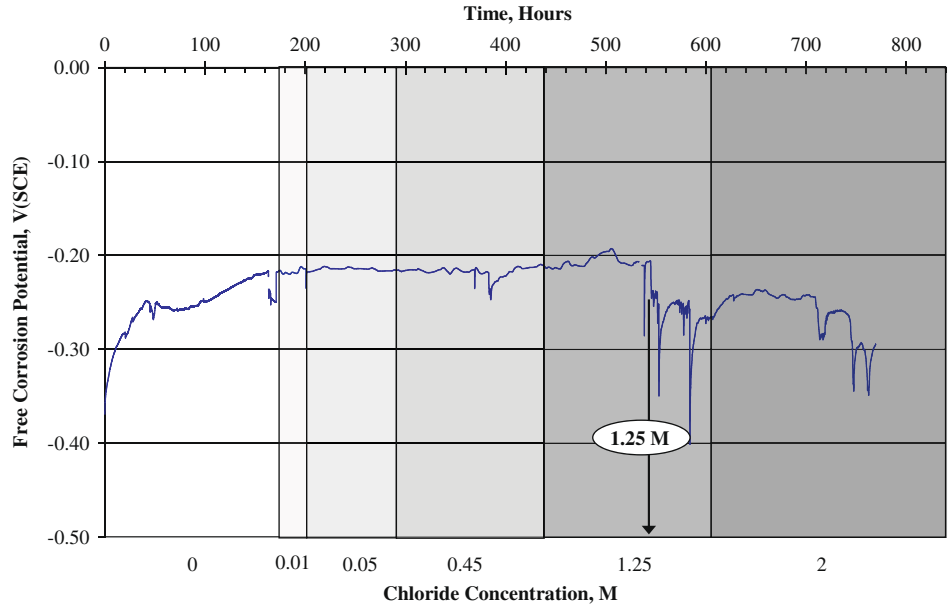

Fig. 5. Average free corrosion potential of three turned-and-polished rebars in CP solution. Shading in the figure corresponds to the increments of chloride addition in Table 3.

lower than the average FCP for the as-received specimens in the same solution (i.e., −169 mV(SCE)).

Figs. 3 and 4 show that the FCP remains relatively constant with increasing chloride concentration until a threshold, $[Cl]_T$, is reached, and then the FCP decreases sharply: the threshold chloride concentrations are 0.1 M and 0.05 M for the CP and the CH solutions, respectively.

The FCP of the turned-and-polished specimens in the CP solution as a function of chloride concentration is shown in Fig. 5. In this case, the threshold occurs at higher chloride concentrations, and the FCP does not fluctuate as much for chloride concentrations above the threshold when compared with the corresponding results for the as-received specimens shown in Fig. 3. The chloride threshold of the polished rebar specimens is approximately 1.25 M, which is significantly higher than the 0.1 M threshold observed for the as-received specimens in the same solution (Fig. 3). This result is consistent with earlier work that has shown polishing increases the chloride threshold of rebar in concrete [6,8,29].

4.2. LPR results

Polarization resistance was determined from the slope of the polarization curve (voltage versus current) for applied voltages of ±15 mV relative to the FCP. The polarization resistances of the rebar specimens measured with LPR are shown in Fig. 6. The chloride thresholds of as-received rebar in the CP and CH solutions are

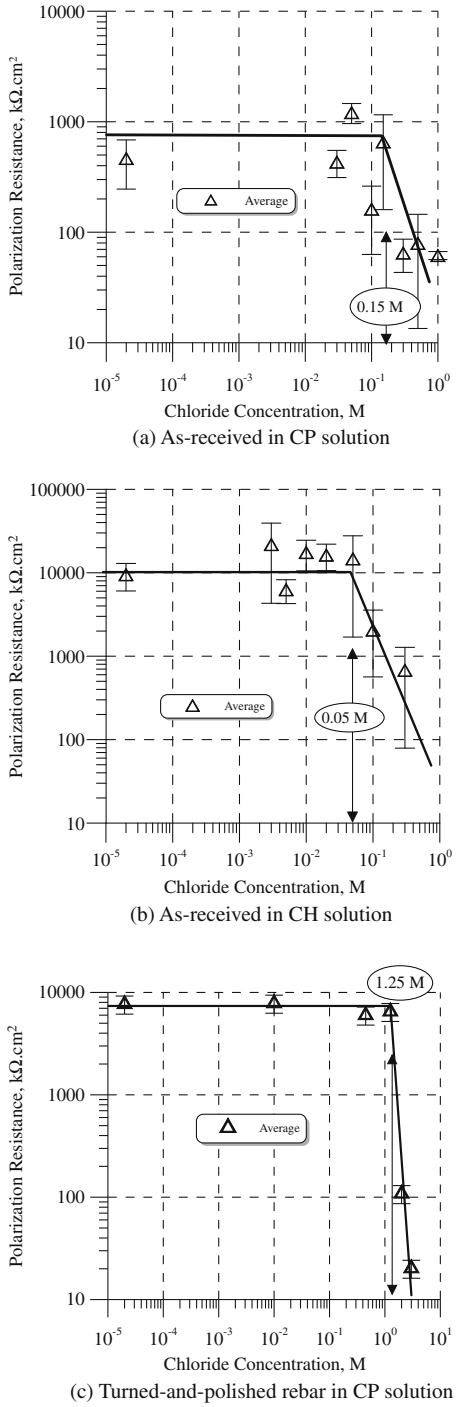

Fig. 6. Polarization resistance of rebar samples obtained by LPR. Note that the data for as-received rebar are more scattered about the trend lines when compared with the data from the turned-and-polished specimens.

0.15 M and 0.05 M, respectively. The threshold for the turned-and-polished specimens in the CP solution is 1.25 M.

4.3. EIS results

Fig. 7 shows distinctly different Bode and Nyquist plots for a typical as-received specimen in the CH solution containing chloride at concentrations below (Fig. 7(a)), and above (Fig. 7(b), the threshold value. Below the chloride threshold, the impedance (Z) increases with decreasing frequency, as shown in the Bode plot on the left of Fig. 7(a). Above the chloride threshold the impedance is relatively constant at low frequencies in the Bode plot of Fig. 7(b), and the Nyquist plot changes from 'linear' in Fig. 7(a) to 'semicircular' in Fig. 7(b). These EIS spectra are typical of passivated and depassivated rebar [8].

Modelling of the EIS results to equivalent electrical circuits was used to reduce the data shown in Fig. 7. Fig. 8 shows the equivalent circuit model that was used [8,27,40–44]. In this model, R_s is the solution resistance (~100 Ω), R_p is the polarization resistance and C_{CPE} is a constant phase element. Using Gamry Echem Analyst V5.3 software, the model parameters were determined by nonlinear least-squares fitting of the real and imaginary components of the impedance to the functional forms derived from the equivalent circuit model.

The ability of the model to reproduce the measured spectra was evaluated with the goodness-of-fit, E^2, defined in the Gamry Echem Analyst software (V5.3) [45,46].

$$E^2 = \frac{\sum_{i=1}^{n}\left[\frac{(y_i - f(v_i))^2}{y_i^2}\right]}{n-m} \quad (1)$$

where y_i is the measured impedance at the ith frequency, v_i; $f(v_i)$ is the impedance calculated from the model; n is the number of data points; and m is the number of adjustable parameters in the model. The standard-deviation errors in the measured impedances are assumed to be constant fractions of the measurements, i.e., $\sigma_i = \varepsilon . y_i$. Hence, the goodness-of-fit, E^2, can be related to the reduced chi-square error, χ^2:

$$E^2 = \varepsilon^2 . \chi^2 \quad (2)$$

Repeated EIS measurements on the same specimen showed reproducibility approaching 6%, however, measurements on triplicate specimens varied up to 15%; hence in this study, ε is assumed to be 0.15. For each spectrum there are 80 data points and 4 model parameters, therefore 76 degrees of freedom. Typical χ^2 values were 1.3 and thus P values were less than 0.05.

Determined polarization resistances of as-received rebar as a function of chloride concentration are shown in Fig. 9. The polarization resistances in this figure are relatively constant as chloride concentration is increased until a threshold value is reached, after which the resistances drop significantly. The thresholds for as-received rebar are 0.15 M and 0.05 M in the CP and the CH solutions, respectively. The polarization resistance of turned-and-polished rebar in the CP solution are shown in Fig. 10. The chloride threshold is 1.25 M.

The magnitudes of the polarization resistances obtained from EIS are generally higher than those from LPR measurements; however, a strong correlation exists between the two. Thus, both measurements are able to capture the chloride threshold. The relationship between the polarization resistances measured by EIS, R_p^{EIS} (kΩ cm²), and by LPR, R_p^{LPR} (kΩ cm²), can be expressed as:

$$\ln(R_p^{LPR}) = 0.90 \times \ln(R_p^{EIS}) + 0.31 \quad (3)$$

with an R^2 value of 0.97.

4.4. AP results

Anodic polarization curves taken before chloride addition, reported as the average of three replicates, are shown in Fig. 11(a) for the CP and CH solutions. In Fig. 11, FCP is the starting potential for the scan, and i_p is the passive current density corresponding to the inflection point of the anodic polarization curve for the forward scan. The repassivation potential (E_{rp}) is the potential in the backward scan when the applied potential is removed. The forward and backward scan directions are identified by arrows. As the chloride

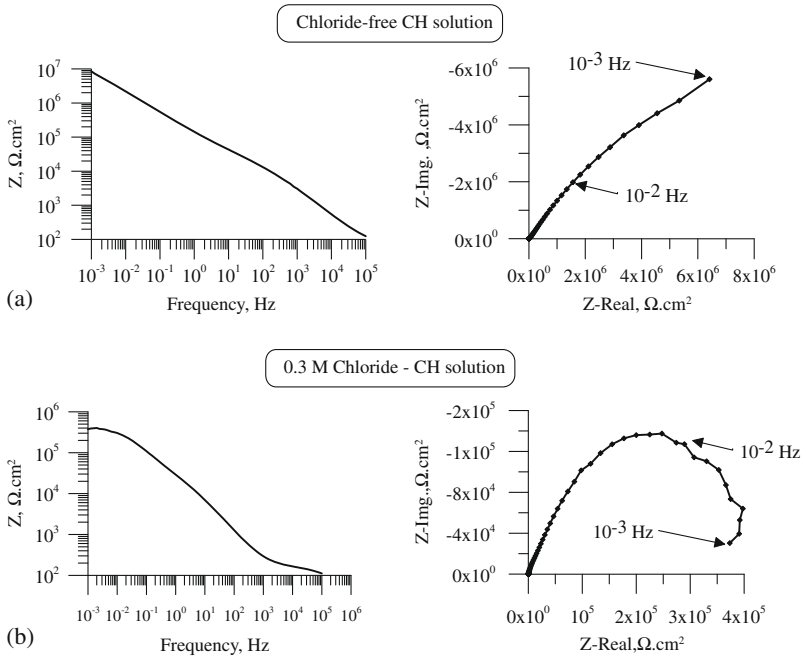

Fig. 7. Typical EIS results obtained for an as-received rebar sample in the CH solution with chloride concentrations (a) below and (b) above the chloride threshold.

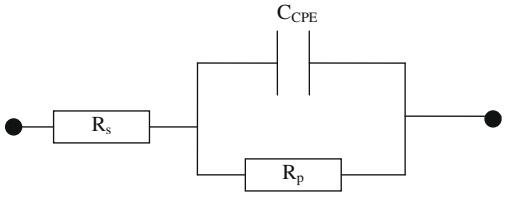

Fig. 8. Equivalent electrical circuit (Randles circuit) used to model the EIS spectra.

concentration in the solution is increased, a pitting potential (E_p) can be defined in the forward scan as the potential corresponding to the sharp increase in current density that is accompanied by the formation of pits on the rebar surface (see Fig. 11(b)).

If the potential is not high enough during the forward scan to cause pitting, then the repassivation potential (E_{rp}) is higher than the initial FCP (Fig. 11(a)), which is generally explained to be because of the growth of a thicker, more protective, oxide during the anodic scan. On the other hand, if pitting does occur, then E_{rp} is lower than the initial FCP as shown in Fig. 11(b). In this case, pitting results in local destruction of the oxide so that it is less protective when the applied anodic potential is removed. Thus, the occurrence of pitting can be determined by comparing the magnitude of E_{rp} with initial FCP.

For the turned-and-polished specimens in the CP solution, pitting could not be observed until large amounts of chloride were added; for these specimens, the average pitting potential was −512 mV(SCE), which occurred after 1.25 M chloride addition. The average FCP and the passive current density (i_p) for as-received rebar specimens after the formation of stable passive films were −169 mV(SCE) and 1 μA/cm² for the CP solution, and −156 mV(SCE) and 0.02 μA/cm² for the CH solution (Figs. 3 and 4). The pitting potentials identified in Fig. 11(b) decrease as the chloride concentration increases. In addition, the pitting potential of rebar in CP is higher than in CH.

A relationship between pitting potential and chloride concentration was obtained by fitting to a logarithmic function of chloride

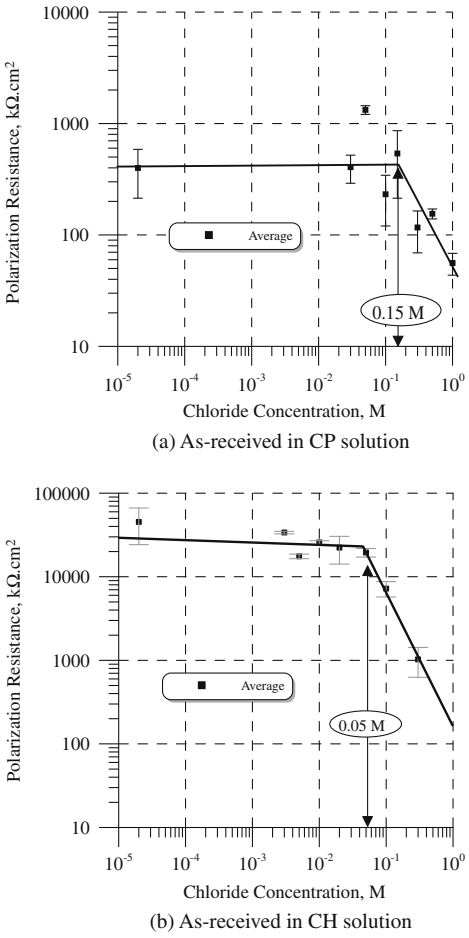

Fig. 9. Polarization resistance (R_p) determined from EIS measurements and equivalent circuit modelling for as-received rebar samples. Note that the data for as-received rebar are more scattered about the trend lines when compared with the data from the turned-and-polished specimens as illustrated in Fig. 10.

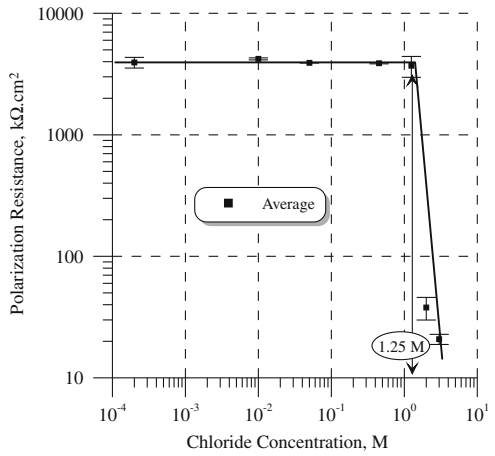

Fig. 10. Polarization resistance (R_p) determined from EIS measurements and equivalent circuit modelling for turned-and-polished rebar samples in CP solution.

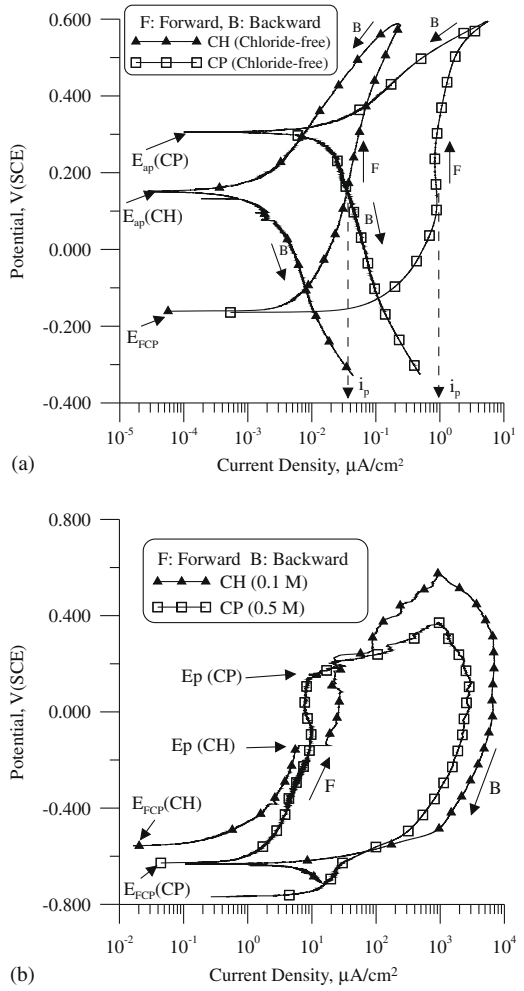

Fig. 11. Anodic polarization curves of as-received rebar in CH and CP solutions (a) without chloride, (b) with chloride.

concentration [10,39,47–52]. The results shown in Fig. 12 give a reasonable correlation with R^2 values of 0.92 and 0.83 for the CH and CP solutions, respectively.

Assuming that pitting occurs once the FCP exceeds the pitting potential, the pitting threshold, $[Cl]_{AP}$ (M), can be calculated using the equations shown in Fig. 12 as follows:

$$-0.156 = -0.51 \times \log([Cl]_{AP}) - 0.44 \Rightarrow [Cl]_{AP} = 0.28\,M \quad (CH\ solution) \tag{4}$$

$$-0.169 = -0.58 \times \log([Cl]_{AP}) - 0.18 \Rightarrow [Cl]_{AP} = 0.96\,M \quad (CP\ solution) \tag{5}$$

Note that the pitting thresholds are higher than the threshold concentrations for depassivation determined by the other methods described previously.

5. Discussion

5.1. Chloride threshold determination technique

The chloride thresholds for depassivation obtained by the different electrochemical techniques used in this study are presented in Table 4. The thresholds determined by FCP, EIS and LPR are similar and much smaller than the chloride thresholds for pitting determined with AP. Similar observations have been reported by Li and Sagues [39]. The AP thresholds are higher because the damaging effect of chloride is offset by the formation and repair of the oxide by the applied anodic potential. Because applied potentials are not routinely used in service, the threshold values obtained from the FCP, EIS and LPR techniques should provide more representative chloride thresholds for rebar in service conditions.

5.2. The effect of solution

The chloride threshold values for as-received rebar specimens in the CP solution were consistently 2–3 times higher than those in the CH solution. This is consistent with earlier work showing chloride thresholds increase as the pH of the solution increases [3,6,8]. In this study, we observed 2–3 times higher thresholds in CP (pH 13.3) compared with CH (pH 12.5), but, this increase is lower than expected: larger changes in thresholds (up to 10 times) have been reported in previous studies for similar pH variations [7,8,53]. However, in these studies, the simulated pore solutions did not contain sulphate ions. Chloride thresholds tend to be lower in solutions with sulphate ions [10,25], and the passive films grown in the presence of sulphate ions have different characteristics [16,54]. The current study re-emphasizes the importance of the composition of the simulated pore solutions in electrochemical studies of rebar corrosion.

5.3. The effect of rebar surface condition

The chloride thresholds measured by FCP, EIS, and LPR are all lower for as-received rebar when compared with turned-and-polished rebar. Li and Sagues reported similar results for rebar specimens that had been sandblasted to remove the mill-scale [8]. Fig. 13 shows pitting potentials determined in the current study, and those from previous work, in terms of the $[Cl^-]/[OH^-]$ concentration ratio. Generally, modifying the rebar surfaces leads to higher chloride thresholds. The implication is that if the goal of an experiment is to determine thresholds that will be representative for service-life-based design and end-of-life calculations, then any surface modification – turning, polishing, sandblasting – should be avoided.

The significance of surface condition can be further demonstrated with reference to Figs. 6, 9 and 10. Compared with the turned-and-polished rebar, the as-received rebar showed greater variability in polarization resistance. For example, in the figures the data for as-received rebar are more scattered about the trend lines when compared with the data from the turned-and-polished specimens. Similar behaviour can be observed in the FCP above the

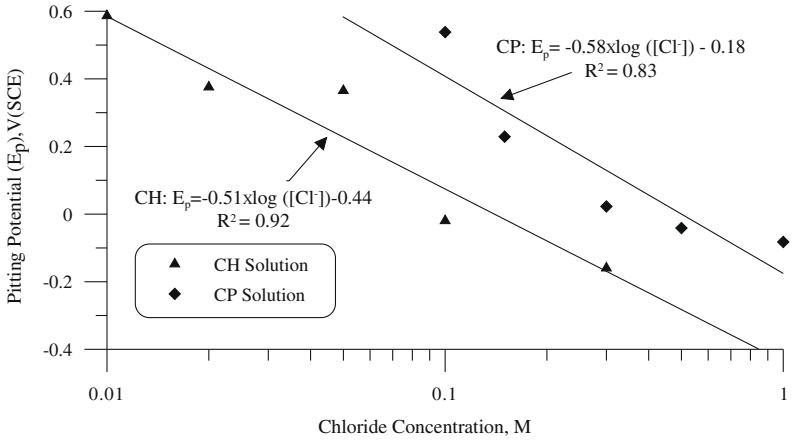

Fig. 12. Pitting potential of as-received rebar in the CH and CP solution as function of chloride.

Table 4
Chloride thresholds obtained by different electrochemical techniques.

Rebar surface preparation	Solution (Table 2)	Chloride threshold, $[Cl]_T$ (M)			
		FCP	EIS	LPR	AP*
As-received	CP	0.05–0.1	0.1–0.15	0.1–0.15	0.96
As-received	CH	0.02–0.05	0.02–0.05	0.02–0.05	0.28
Turned-and-Polished	CP	0.45–1.25	0.45–1.25	0.45–1.25	N/A

FCP, free corrosion potential; EIS, electrochemical impedance spectroscopy; LPR, linear polarization resistance; AP, anodic polarization.
* Calculated from the AP results as shown in Section 4.4 ($[Cl]_{AP}$).

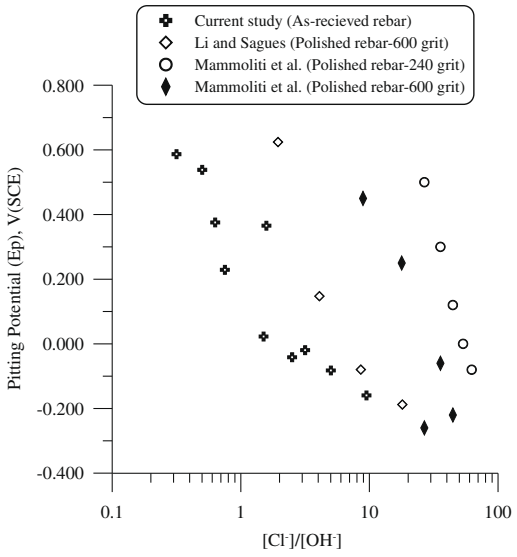

Fig. 13. Pitting potentials from the current study and those reproduced from Li and Sagues [39] and Mammoliti et al. [6]. As-received rebar specimens pit at lower $[Cl^-]/[OH^-]$ ratios than polished rebar specimens.

threshold for the specimens in the CP solution; in Figs. 3 and 5 the FCP for the as-received specimens fluctuates much more than it does for the turned-and-polished specimens. The inference is that the turned-and-polished surfaces are uniformly the same everywhere, whereas the as-received surfaces are locally much more diverse and complex.

The importance of the as-received rebar surface suggests an explanation for the wide range and uncertainty of reported in-service chloride thresholds measured in similar concrete types under the same environmental conditions [1,2]. The variability associated with the chloride thresholds may be attributed to the variability in the surface characteristics of the steel resulting from the variability in fabrication and production; there is usually no strict quality control for the mill-scale on rebar. Preliminary studies implicate the mill-scale as part of the explanation for the lower thresholds for as-received rebar [55].

5.4. Observations before depassivation

The average passive current densities (i_p) of rebar measured in the AP tests before chloride addition were significantly different in the CP and CH solutions: 1 μA/cm^2 and 0.02 μA/cm^2, respectively, as shown in Fig. 11(a). In addition, the polarization resistances measured by LPR and EIS were higher in CH solutions (Figs. 6, 9 and 10). Lower passive current densities and higher polarization resistances for the passive films in the CH solution may suggest more resistance to corrosion. However, the passive film in CH solution had a lower chloride threshold, which shows that the resistance of the passive film to corrosion does not necessarily mean that the film will be more resistant to chloride.

The FCP does not change significantly with chloride addition up to threshold concentrations, as can be seen in Figs. 3–5. Similarly, polarization resistances shown in Figs. 9 and 10 remain relatively constant until the chloride thresholds and then drop. Thus, chloride is not systematically changing the electrical properties of the film. For instance, if chloride were thinning the oxide film or making it more porous, then we should observe the oxide film resistance decrease; however, it remains relatively constant below the threshold. Similar conclusions were drawn for iron depassivation due to chloride in mildly alkaline solution [56]. Hence, chloride-induced depassivation of rebar in highly alkaline solutions is more likely caused by critical chemical conditions that lead to depassivation. These critical conditions occur at lower chloride

concentrations, as measured in the bulk solution, for as-received specimens than turned-and-polished specimens, which suggests that the local chemistry at the surface of the as-received rebar may be different from that in the bulk solution.

5.5. Final thoughts

Reconciling measurements of chloride thresholds for black steel rebar are complicated by a number of factors that include differences in specimen surface preparations, differences in synthetic pore solutions, and different experimental methods. However, even when the same experimental methods and specimen preparation techniques are used, there is a high degree of variability in the chloride threshold values. This suggests that in addition to reporting chloride thresholds, some indication of the variability is also required.

Fig. 14 shows the cumulative probability of depassivation, P_D, which is defined as the ratio of the number of depassivated specimens to the total number of specimens, $N = 24$, for a given chloride concentration. (A specimen was defined to be depassivated when its FCP dropped below −250 mV(SCE). This value was chosen because pits initiate on the surface for specimens when FCP is lower than −250 mV(SCE). Varying this value by 50 mV did not affect the probability distribution.) Fig. 14 shows that the probability of depassivation increases with chloride addition, and that the probabilities are higher in the CH solution than in the CP solution.

The results shown in Fig.14, were fitted to the cumulative log-normal probability distribution function:

$$P_D = 0.5\left(1 + \mathrm{erf}\left(\frac{\log[Cl] + pCl_T}{\sigma\sqrt{2}}\right)\right) \quad (6)$$

where [Cl] (M) is the chloride concentration, σ (M) is the logarithmic standard deviation and pCl_T (M) is defined as

$$pCl_T = -\log[Cl]_T \quad (7)$$

In the regressions each datum was weighted by the squared inverse of its estimated error, which was calculated in accord with Poisson counting statistics. The pCl_T and σ obtained for the CH solution were 1.16 ± 0.07 and 0.45 ± 0.11, respectively, whereas for the CP solution, pCl_T and σ were 0.74 ± 0.1 and 0.4 ± 0.14, respectively. The P values for the regressions were less than 0.05.

These values of pCl_T are the most probable logarithmic chloride thresholds (i.e., the modes of the distributions), as well as the medians and means because the probability of depassivation is distributed symmetrically (i.e., normally) in terms of the logarithm of chloride concentration. However, if instead the independent variable was simply chloride concentration, the distributions would be skewed, and the mode, median and mean would no longer be the same: the modes for the CH and CP solution are 0.023 M and 0.08 M, respectively; the medians for the CH and CP solution are 0.07 M and 0.18 M, respectively; and the respective means are 0.12 M and 0.29 M. This begs the question: which of these means, modes and medians should be used to characterize the threshold? The answer is that any of these will work, as long as one other parameter is included to complete the description of the distribution, (i.e., some parameterization of the width/variability). This suggests that simple averages of chloride threshold measurements might not provide reliable indicators of depassivation. For our purposes, pCl_T and σ, and Eq. (6), were used to predict the probability of exceeding the chloride threshold.

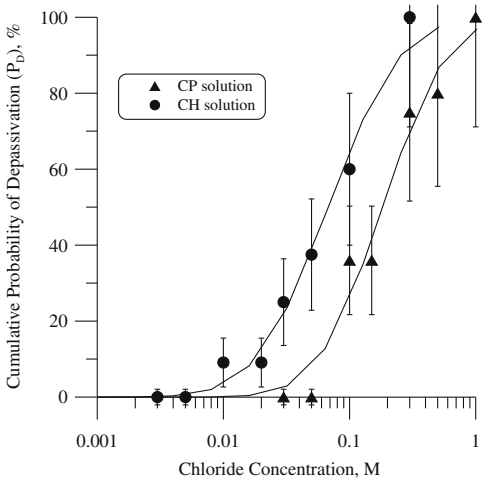

Fig. 14. Cumulative probability of depassivation for as-received rebar as a function of chloride concentration. The curves in the figure were calculated from the cumulative log-normal probability distribution function, equation 6, and values of pCl_T and σ, as described in Section 5.5.

6. Conclusions

In this study, we used FCP, LPR, EIS and AP to determine chloride thresholds in an electrochemical cell in which short specimens of as-received rebar were immersed in simulated concrete pore solution, and surrounded by a co-axial counter electrode. We report a method to coat the cut ends of the rebar specimens that effectively eliminates confounding crevice corrosion.

Two types of rebar surface condition were studied: as-received and turned-and-polished. Modification of the rebar surfaces, by turning and polishing, led to higher depassivation thresholds: the as-received specimens had lower chloride thresholds. The implication is that if the goal is to determine thresholds that will be representative for service-life-based design and end-of-life calculations, then any experimental surface modification should be avoided. Modifying the rebar surface also led to reduced variability in polarization resistance, and reduced fluctuations in FCP above the depassivation threshold. These results of surface modification suggest that the variability associated with reported chloride thresholds may be attributed to the variability in the surface characteristics of the rebar resulting from the variability in fabrication and production.

The variability in chloride thresholds for as-received rebar was found to be well represented by a log-normal distribution. This suggests that simple averages of chloride threshold measurements, without reference to the underlying distribution, might not provide reliable indicators of depassivation. In this study, probabilities of depassivation are reported in addition to chloride thresholds.

The relative constancy of electrochemical measurements below the thresholds, and the dependence of the thresholds on the state of the surface, suggests that chloride-induced depassivation of rebar in highly alkaline solutions is likely caused by the occurrence of local critical chemical conditions at the surface of the rebar.

Acknowledgments

This research was supported by a Grant from the Natural Sciences and Engineering Research Council (NSERC) of Canada along with technical and financial support of CANMET-MTL laboratories, through the Resource for Innovation of Engineered Materials (RIEM) program. Both contributions are gratefully acknowledged. We also would like to thank Brian Foo for his contributions during the production of some of the figures in this paper.

References

[1] G.K. Glass, N.R. Buenfeld, The presentation of the chloride threshold level for corrosion of steel in concrete, Corros. Sci. 39 (5) (1997) 1001–1013.

[2] C. Alonso, C. Andrade, M. Castellote, P. Castro, Chloride threshold values to depassivate reinforcing bars embedded in a standardized OPC mortar, Cem. Concr. Res. 30 (7) (2000) 1047–1055.
[3] V.K. Gouda, Corrosion and corrosion inhibition of reinforcing steel: 1—Immersion in alkaline solution, Br. Corros. J. 5 (1970) 198–203.
[4] S. Goni, C. Andrade, Synthetic concrete pore solution chemistry and rebar corrosion rate in the presence of chlorides, Cem. Concr. Res. 20 (4) (1990) 525–539.
[5] K. Pettersson, Chloride threshold value and the corrosion rate in reinforced concrete, Cem. Concr. Res. 24 (1994) 461–470.
[6] L. Mammoliti, L. Brown, C. Hansson, B. Hope, The influence of surface finish of reinforcing steel and pH of the test solution on the chloride threshold concentration for corrosion initiation in synthetic pore solutions, Cem. Concr. Res. 26 (4) (1996) 545–550.
[7] W. Breit, Kritischer chloridgehalt-untersuchungen an stahl in chloridhaltigen alkalischen LoÈsungen, Mater. Corros. 49 (8) (1998) 539–550.
[8] L. Li, A.A. Sagues, Chloride corrosion threshold of reinforcing steel in alkaline solutions-open-circuit immersion tests, Corrosion 57 (1) (2001) 19–28.
[9] B.H. Oh, S.Y. Jang, Y.S. Shin, Experimental investigation of the threshold chloride concentration for corrosion initiation in reinforced concrete structures, Mag. Concr. Res. 55 (2) (2003) 117–124.
[10] H.E.H. Bird, B.R. Pearson, P.A. Brook, The breakdown of passive films on iron, Corros. Sci. 28 (1) (1988) 81–86.
[11] C.M. Hansson, B. Sorensen, The threshold concentration of chloride in concrete for the initiation of reinforcement corrosion, in: N.S. Berke, V. Chaker, D. Whitting (Eds.), Corrosion Rates of Steel in Concrete, ASTM (STP1065), 1988, pp. 3–16.
[12] S.E. Hussain, Rasheeduzzafar, A. Al-Musallam, A.S. Al-Gahtani, Factors affecting threshold chloride for reinforcement corrosion in concrete, Cem. Concr. Res. 25 (7) (1995) 1543–1555.
[13] M. Thomas, Chloride thresholds in marine concrete, Cem. Concr. Res. 26 (4) (1996) 513–519.
[14] C. Andrade, C.L. Page, Pore solution chemistry and corrosion in hydrated cement systems containing chloride salts: a study of cation specific effects, Br. Corros. J. 21 (1) (1986) 49–53.
[15] O.A. Kayyali, M.N. Haque, The Cl^-/OH-ratio in chloride-contaminated concrete-A most important criterion, Mag. Concr. Res. 47 (1995) 235–242.
[16] P. Ghods, O.B. Isgor, G. McRae, T. Miller, The effect of concrete pore solution composition on the quality of passive oxide films on black steel reinforcement, Cem. Concr. Compos. 31 (1) (2009) 2–11.
[17] R.G. Pilla, D. Trejo, Surface condition effects on critical chloride threshold of steel reinforcement, ACI Mater. J. 102 (2) (2005) 103–109.
[18] J.A. Gonzalez, E. Otero, S. Feliu, W. Lopez, Initial steps of corrosion in the steel/$Ca(OH)_2$Cl system: The role of heterogeneities on the steel surface and oxygen supply, Cem. Concr. Res. 23 (1) (1993) 33–40.
[19] G.K. Glass, N.R. Buenfeld, The inhibitive effects of electrochemical treatment applied to steel in concrete, Corros. Sci. 42 (6) (2000) 923–927.
[20] S. Rasheeduzzafar, E. Hussain, S.S. Al-Saadoun, Effect of tricalcium aluminate content of cement on chloride binding and corrosion of reinforcing steel in concrete, ACI Mater. J. 89 (1) (1993) 3–12.
[21] S.E. Hussain, A.S. Al-Gahtani, Chloride threshold for corrosion of reinforcement in concrete, ACI Mater. J. 93 (6) (1996) 534–538.
[22] G.K. Glass, N.R. Buenfeld, The influence of chloride binding on the chloride induced corrosion risk in reinforced concrete, Corros. Sci. 42 (2) (2000) 329–344.
[23] K.H. Pettersson, Factors influencing chloride induced corrosion of reinforcement in concrete, Durability Build. Mater. Compon. 1 (1996) 334–341.
[24] P.S. Mangat, B.T. Molloy, Factors influencing chloride-induced corrosion of reinforcement in concrete, Mater. Struct. 25 (7) (1992) 404–411.
[25] E.E. Abd El Aal, S. Abd El Wanees, A. Diab, S.M. Abd El Haleem, Environmental factors affecting the corrosion behavior of reinforcing steel III. measurement of pitting corrosion currents of steel in $Ca(OH)_2$ solutions under natural corrosion conditions, Corros. Sci. 51 (8) (2009) 1611–1618.
[26] M. Saremi, E. Mahallati, A study on chloride-induced depassivation of mild steel in simulated concrete pore solution, Cem. Concr. Res. 32 (12) (2002) 1915–1921.
[27] Y.S. Choi, J.G. Kim, K.M. Lee, Corrosion behaviour of steel bar embedded in fly ash concrete, Corros. Sci. 48 (7) (2006) 1733–1745.
[28] L. Li, A.A. Sagues, Chloride corrosion threshold of reinforcing steel in alkaline solutions—effect of specimen size, Corrosion 60 (2) (2004) 195–202.
[29] E. Mahallati, M. Saremi, An assessment on the mill scale effects on the electrochemical characteristics of steel bars in concrete under DC-polarization, Cem. Concr. Res. 36 (7) (2006) 1324–1329.
[30] M. Pour-Ghaz, O.B. Isgor, P. Ghods, The effect of temperature on the corrosion of steel in concrete. Part 1: simulated polarization resistance tests and model development, Corros. Sci. 51 (2) (2009) 415–425.
[31] A.A. Sagues, L. Li, H.W. Pickering, Crevice effect on corrosion of steel in simulated concrete pore solutions, Corrosion 56 (10) (2000) 979–982.
[32] C.L. Page, Ø. Vennesland, Pore solution composition and chloride binding capacity of silica-fume cement pastes, Mater. Struct. 16 (1) (1983) 19–25.
[33] A. Moragues, A. Macias, C. Andrade, Equilibria of the chemical composition of concrete pore solution: I, comparative study of synthetic and extracted solutions, Cem. Concr. Res. 17 (2) (1987) 173–182.
[34] K. Andersson, B. Allard, M. Bengtsson, B. Magnusson, Chemical composition of cement pore solutions, Cem. Concr. Res. 19 (3) (1989) 327–332.
[35] T.D. Marcotte, Characterization of chloride-induced corrosion products that form in steel-reinforced cementitious materials, Ph.D. dissertation, Waterloo University, Canada (2001).
[36] A. Poursaee, C.M. Hansson, Reinforcing steel passivation in mortar and pore solution, Cem. Concr. Res. 37 (7) (2007) 1127–1133.
[37] Standard reference test method for making potentiostatic and potentiodynamique anodic polarization Measurements, ASTM G5-94, Wear and Erosion; Metal Corrosion ASTM vol. 03.02, ASTM, Philadelphia, 1998. pp. 54–64.
[38] H.P. Leckie, A contribution to the applicability of critical pitting potentials, J. Electrochem. Soc. 117 (1970) 1152–1154.
[39] L. Li, A.A. Sagues, Chloride corrosion threshold of reinforcing steel in alkaline solutions-cyclic polarization behaviour, Corrosion 58 (4) (2002) 305–316.
[40] N.S. Berke, M. C. Hicks, Electrochemical methods of determining the corrosivity of steel in concrete, in: R. Baboian, S.W. Dean (Eds.), Corrosion Testing and Evaluation, ASTM (STP1000), 1990, pp. 425–440.
[41] V. Feliu, J.A. González, C. Andrade, S. Feliu, Equivalent circuit for modelling the steel-concrete interface. I. Experimental evidence and theoretical predictions, Corros. Sci. 40 (6) (1998) 975–993.
[42] P. Garcés, M.C. Andrade, A. Saez, M.C. Alonso, Corrosion of reinforcing steel in neutral and acid solutions simulating the electrolytic environments in the micropores of concrete in the propagation period, Corros. Sci. 47 (2) (2005) 289–306.
[43] C.K. Nmai, Multi-functional organic corrosion inhibitor, Cem. Concr. Compos. 26 (3) (2004) 199–207.
[44] G. Trabanelli, C. Monticelli, V. Grassi, A. Frignani, Electrochemical study on inhibitors of rebar corrosion in carbonated concrete, Cem. Concr. Res. 35 (9) (2005) 1804–1813.
[45] W.S. Tait, K.A. Handrich, S.W. Tait, J.W. Martin, Analyzing and interpreting electrochemical impedance spectroscopy data from internally coated steel aerosol containers, in: J.C. Scully, D.C. Silverman, M.W. Kendig (Eds.), Electrochemical Impedance Analysis and Interpretation, ASTM (STP 1188), 1993, pp. 428–437.
[46] S. Siegel, N.J. Castellani Jr, Nonparametric Statistics for the Social Sciences, MacGraw-Hill, New York, 1988.
[47] L. Freiman, Y. Kolotyrkin, Iron passivation potential and solution compositin, Protection of Metals 5 (2) (1969) 113–121.
[48] M. Janik-Czachor, An assessment of the processes leading to pit nucleation on iron, J. Electrochem. Soc. 128 (12) (1981) 513C–519C.
[49] K.E. Heusler, L. Fischer, Kinetics of pit initiation at passive iron, Mater. Corros. 27 (8) (1976) 551–556.
[50] H.H. Strehblow, B. Titze, Pitting potential and inhibition potentials of iron and nickel for different aggressive and inhibiting anions, Corros. Sci. 17 (6) (1977) 461–472.
[51] M.G. Alvarez, J.R. Galvele, The mechanism of pitting of high purity iron in NaCl solutions, Corros. Sci. 24 (1) (1984) 27–48.
[52] M. Ergun, A.Y. Turan, Pitting potential and protection potential of carbon steel for chloride ion and the effectiveness of different inhibiting anions, Corros. Sci. 32 (10) (1991) 1137–1142.
[53] D.A. Hausmann, Steel corrosion in concrete – how does it occur, Mater. Prot. 6 (11) (1967) 19–23.
[54] J. Gui, T.M. Devine, The influence of sulphate ions on the surface enhanced Raman spectra of passive films formed on iron, Corros. Sci. 36 (3) (1994) 441–462.
[55] P. Ghods, O.B. Isgor, G. McRae, G.P. Gu, J. Li, Effect of surface condition on the chloride-induced depassivation of rebar in concrete, in: 12th International Conference on Fracture (ICF), Ottawa, Canada CD proceeding, 2009.
[56] R. Goetz, B. MacDougall, M.J. Graham, An AES and SIMS study of the influence of chloride on the passive oxide film on iron, Electrochim. Acta 31 (10) (1986) 1299–1303.